AIAA 96-0764

High Resolution Euler Solvers Based on the Space-Time Conservation Element and Solution Element Method

X.Y. Wang, C.Y. Chow
University of Colorado
Boulder, CO
and
S.C. Chang
NASA Lewis
Cleveland, OH

34th Aerospace Sciences Meeting & Exhibit
January 15-18, 1996 / Reno, NV

HIGH RESOLUTION EULER SOLVERS BASED ON THE SPACE-TIME CONSERVATION ELEMENT AND SOLUTION ELEMENT METHOD

Xiao-Yen Wang,* Chuen-Yen Chow†
Department of Aerospace Engineering, University of Colorado, Boulder, CO 80309
Sin-Chung Chang‡
NASA Lewis Research Center, Cleveland, OH 44135

Abstract

The 1-D, quasi 1-D and 2-D Euler solvers based on the method of space-time conservation element and solution element are used to simulate various flow phenomena including shock waves, Mach stem, contact surface, expansion waves, and their intersections and reflections. Seven test problems are solved to demonstrate the capability of this method for handling unsteady compressible flows in various configurations. Numerical results so obtained are compared with exact solutions and/or numerical solutions obtained by schemes based on other established computational techniques. Comparisons show that the present Euler solvers can generate highly accurate numerical solutions to complex flow problems in a straightforward manner without using any ad hoc techniques in the scheme.

1. Introduction

The method of space-time conservation element and solution element (to be abbreviated as the CE/SE method) is a new numerical method developed by Chang for solving conservation laws.[1-4] It is different in both concept and methodology from the well-established traditional methods such as the finite difference, finite volume, finite element and spectral methods. It is designed from a physicist's perspective to overcome several key limitations of the traditional methods.

Simplicity, generality and accuracy are weighted in the development of the present method while satisfying the fundamental computational requirements. Its salient properties are summarized briefly as follows. First, the concepts of conservation element and solution element are introduced to enforce both local and global flux conservation in space and time instead of in space only. Second, all the dependent variables and their spatial derivatives are considered as individual unknowns to be solved simultaneously at each grid point. Third, no approximation techniques other than Taylor's series expansion, no monotonous constraints, and no characteristic-based techniques are used in the design of the scheme. Detailed description of this method and the accompanied analysis are referred to Refs. 1 and 2.

Various efficient numerical schemes based on the CE/SE method have been developed for solving different flow problems, especially the problems in the presence of shock waves with discontinuous flow properties. Of those schemes, the one- and two-dimensional time marching Euler solvers are employed here to solve problems involving flow phenomena that are more complex than those shown in Refs. 1 and 2. In addition, a quasi one-dimensional Euler solver is constructed in this work which is aimed at dealing with problems in axisymmetric configurations. Comparisons of the computed results with published data are made to demonstrate the simplicity and accuracy of the present Euler solvers.

Detailed description of the governing equations and CE/SE 1-D, quasi 1-D, 2-D Euler solvers used in the following numerical tests is referred to Ref. 3, while numerical results and discussions are described in details as follows.

2. Numerical Results

2.1) 1-D shock-tube problems

In the 1-D weighted-average Euler α-ϵ scheme used in the numerical tests for the following four shock-tube problems, the parameter ϵ is set as 0.5, while α is 1 except in the first problem where α is 4.

a) The Lax problem

The initial conditions in the region $[-8, 6]$ on the x axis are defined as

$$\rho_l = 0.445, \quad u_l = 0.6989, \quad p_l = 3.5277 \quad x < 0 \quad (1)$$

$$\rho_r = 0.5, \quad u_r = 0.0, \quad p_r = 0.571 \quad x \geq 0 \quad (2)$$

*Graduate Research Assistant.
†Professor, AIAA Associate Fellow.
‡Senior Scientist.

The numerical solution at $t = 100\Delta t$ obtained by using the present scheme, under the same computational conditions (CFL=0.95 and $\Delta x = 0.1$) as those used in Ref. 5, is shown with the exact solution represented by solid lines in Fig. 1. Comparisons were made by Harten[5] to appraise four numerical schemes, namely, the ROE, LW (Lax-Wendroff), ULT1, and ULT1C schemes, which were used to solve the same problem. The last two are the TVNI finite-difference schemes designed by Harten. The numerical results plotted in Figs. 2(a)–(d) of Ref. 5 are not reproduced here. Among the four solutions, the LW solution is the worst showing serious oscillations near the shock discontinuity. In the ROE solution, the oscillations disappear but up to four grid points are needed to resolve a shock wave, while a significant smear is found either near the contact surface or within the expansion fan. Much improvement is revealed in the ULT1 solution, which resolves a shock discontinuity with only 2 grid points and shows an excellent agreement with the exact solution except in the diffusive region near the contact surface. The ULT1 solution closely resembles the solution plotted in Fig. 1 obtained by use of the present Euler solver. Harten showed that a further refinement can be obtained by using the higher order accurate ULT1C scheme.

b) The Sjogreen problem

This problem is taken from Ref. 6, whose initial conditions are

$$\rho_l = 1.0, \quad u_l = -2, \quad p_l = 0.4 \quad 0 < x < 0.5 \quad (3)$$

$$\rho_r = 1.0, \quad u_r = 2, \quad p_r = 0.4 \quad 0.5 \leq x < 1.0 \quad (4)$$

The initial velocity discontinuity causes two rarefaction waves to propagate in opposite directions, leaving in between a region of high vacuum. It was mentioned[7] that several Godunov-type schemes failed in this problem due to the extremely low pressure in the middle region. The CE/SE solution at $t = 50\Delta t$ based on 100 grid points and $\Delta t = 0.002$ is shown in Fig. 2, in which the exact solution is represented by solid lines. It can be seen that the present solution agrees very well with the exact solution, without showing negative pressure values in the middle region. The solution displays an accuracy which is comparable to that obtained by Xu et al.[7] using a gas-kinetic scheme with 200 grid points.

c) The Shu-Osher problem

Examined in this problem is the interaction of a moving shock of $M_s = 3$ with a sinusoidal density wave.[8] The initial conditions in the region $[-5, 5]$ are described as

$$\rho_l = 3.857, \quad u_l = 2.629, \quad p_l = 10.333 \quad x < -4 \quad (5)$$

$$\rho_r = 1 + 0.2\sin 5x, \quad u_r = 0, \quad p_r = 1 \quad \text{otherwise} \quad (6)$$

This problem does not have an exact solution. Several upwind schemes have been used to solve this problem to compare their abilities in resolving the peaks appeared in the solution.[9] The CE/SE solution at t=1.8 obtained by using 800 grid points with $\Delta t = 0.0015$ (CFL=0.582) is shown in Fig. 3. The present solution is comparable to those obtained in Ref. 9 by using the TVD1 and TVD2 schemes with the same number of grid points.

d) The Woodward-Colella problem

This problem, concerning the interaction of two blast waves in a close-ended tube, was proposed by Woodward and Colella without an exact solution.[10] The initial conditions are

$$\rho_l = 1.0, \quad u_l = 0, \quad p_l = 1000 \quad x < 0.1 \quad (7)$$

$$\rho_m = 1.0, \quad u_m = 0, \quad p_m = 0.01 \quad 0.1 \leq x < 0.9 \quad (8)$$

$$\rho_r = 1.0, \quad u_r = 0, \quad p_r = 100 \quad 0.9 \leq x \leq 1.0 \quad (9)$$

The two ends are at $x = 0$ and $x = 1$ where the reflecting boundary conditions are imposed. Detailed reflecting boundary conditions used in the present scheme are referred to Ref. 4. The CE/SE solution at t=0.038 based on 800 grid points with $\Delta t = 1.25 \times 10^{-5}$(CFL=0.3524) is shown in Fig. 4. The flowfield at t=0.038 contains three contact surfaces and two shock waves. It can be seen that the contact surfaces are much smeared than the shock discontinuities. A comparison with the numerical solutions obtained by using AUSM$^+$, Roe, Van leer, AUSMDV and AUSM$^+$-w splitting schemes for the same problem shown in Fig. 5 of Ref. 11 reveals that the CE/SE solution is at least of the same accuracy.

It has been demonstrated that the present 1-D Euler solver can generate highly accurate solutions to shock-tube problems involving various discontinuities, even though it does not need the implement of monotonous restraints, TVNI, and entropy conditions as did in Ref. 5. This simple scheme can be used without difficulty to solve any 1-D problems governed by Euler equations.

2.2) A quasi 1-D nozzle flow

An axisymmetric nozzle with cross-sectional area $A(x) = 1.398 + 0.347\tanh(0.8x - 4)$ described in Refs. 5 and 12 is reconsidered here. Numerical solutions obtained by use of the quasi 1-D Euler solver for CFL=0.9 with 20 and 32 grid points are shown in Figs. 5 and 6, respectively. The present solution with 20 grid points is at least as good as those obtained by ROE and ULT1 schemes shown in Fig. 6 of Ref. 5 with the same number of grid points, while

the present solution with 32 grid points is better than the ULT1 solution with 50 grid points.

2.3) 2-D supersonic flow past a step

Consider the supersonic channel flow past a step depicted in Fig. 7(a). The flow exhibits complicated phenomena which include Mach stem, slip surface, shock wave, expansion fan, and their interactions and reflections. This is a standard benchmark problem in the literature. It was used to test Harten's TVNI ULT1C scheme,[5] Giannakouros and Karniadakis' spectral element-FCT method,[13] and Van Leer's ultimate conservative difference scheme.[14] It was also adopted by Woodward and Colella[10] to compare the accuracy of different numerical methods in handling a shock discontinuity. This problem is solved again here to demonstrate the robustness of the CE/SE method.

The 2-D weighted-average Euler a-ϵ scheme with $\epsilon = 0.5$ and $\alpha = 1$ is used in this numerical test. The grid distribution shown in Fig. 7(b) indicates that no grid point is placed at the upper corner of the step to avoid the singular flow behavior there. The freestream condition is set at the inlet, while the condition at the exit is extrapolated from the interior. The reflective boundary condition is imposed on solid walls. Detailed description of boundary conditions can be found in Ref. 3.

The density contours in the solutions obtained by the present Euler solver with 61x21, 121x41 and 241x81 grid points are shown in Fig. 8. Similar contour plots are displayed in Figs. 7(a)-(g) of Ref. 10 based on six selected numerical schemes. According to Ref. 10, the ranking of these six methods in terms of accuracy is as follows: PPM(both PPMLR and PPMDE), MUSCL, ETBFCT, BBC, MacCormack's scheme, and Godunov's scheme.

Comparisons under the same computational conditions (CFL=0.8, $\Delta t = 0.0025$ for 241x81 grid) show that the present solution is as good as those obtained by the accurate MUSCL and PPMDE schemes and is much better than Godunov's solution. A direct comparison cannot be made with other mentioned schemes because of their different time step sizes and CFL numbers. The Mach stem, triple point, slip surface, expansion fan at the corner, and the interaction between the reflected shock with rarefaction waves are accurately simulated in the present numerical solutions.

2.4) A 2-D blast flowfield

Considered here is a blast flowfield generated by an open-ended cylindrical shock tube, which was simulated in Ref. 15 using a TVD finite volume method with numerical techniques for controlling artificial compressibility and dissipation. The flowfield involves complicated phenomena including vortex, blast wave, rarefaction wave, normal shock and their mutual interactions. The early time development of vortex and shock diffraction and the subsequent flow evolution were simulated in Ref. 15 up to 1.5 msec to show a fair comparison with experimental data. This problem is solved here on cartesian coordinates using the CE/SE method to demonstrate its versatility.

The two-dimensional shock tube configuration adopted for numerical computation is depicted in Fig. 9, in which the blank space is used to represent the solid tube wall above the plane of symmetry on the x axis. Displayed schematically in the figure are some representative grid points. A shock wave is created by the sudden removal of a diaphragm at the lip of the tube which separates a compressed fluid in region 2 inside the tube from the surrounding stagnant fluid in region 1. The initial conditions are described by

$$p_1 = 1/1.4, \quad \rho_1 = 1.0, \quad u_1 = 0.0, \quad v_1 = 0.0 \quad (10)$$

$$p_2 = 2.443, \ \rho_2 = 2.28, \ u_2 = 0.982, \ v_2 = 0.0 \quad (11)$$

The 2-D Euler solver with $\epsilon = 0.5$ and $\alpha = 1$ is used to compute the flowfield with $\Delta t = 0.0025$ on a mesh of 49x97 grid points. The nonreflective boundary condition is set at the inlet, outlet, and upper boundary of the computational domain, while the reflective boundary condition is set on the x axis and at all tube walls.

Qualitative agreements between computed and measured positions of the vortex center (estimated from Fig. 15 of Ref. 15) at six time levels are revealed in Fig. 10. A quantitative comparison is not feasible due to the fact that the experiment was performed in an axisymmetric configuration whereas the computation was in 2-D. However, at an early stage the measured vortex positions are correctly predicted by the 2-D code.

The velocity vector fields at six time levels are plotted in Fig. 11 to show the formation and movement of both the vortex and blast wave. The vortex can be recognized by its characteristic revolving flow pattern and the blast wave is represented by a shallow banded curve. The computed flow features can be detected in photographs taken at different time steps.[15] Our numerical results with 4753 grid points uniformly distributed in the computational domain are comparable to those reported in Ref. 15 based on a finite volume method containing 7377 cells, with much smaller cells densely distributed in the neighborhood of the tube exit.

After this test, the 2-D blast flowfield generated by the same initial conditions is simulated to further test the robustness of the present Euler solver. The computational domain is enlarged to $-1 \leq x \leq 3$ and $0 \leq y \leq 3$, which is the same as that of the axisymmetric flowfield simulated in Ref. 15. The boundary conditions are the same as those described previously except the upper surface is now replaced by a solid wall. The reflection of the blast wave from the upper surface causes additional flow phenomena that were not observed in the experiment.

To show the time history of flow development, numerical solutions at eight time levels obtained using 161x121 grid points are shown in Figs. 12 and 13, in which the pressure and density contours ranging from 0 to 5.88 with a constant interval of 0.049 are plotted. The sequential plots reveal that as the blast wave initiated from the open end of the shock tube propagates away, a vortex is developed at the lip of the tube wall, which moves downstream with an ascending motion. When the blast wave reaches the upper wall, it is reflected as shown in the plot at t=1.0 msec. In the meantime on the tube axis a normal shock is formed ahead the vortex and is moving slowly in the downstream direction, while a jet shear layer is created at the lip of the shock tube. At t=1.5 msec, the portion of the blast wave that is reflected from the upper wall is shown to move toward the vortex. After passing the vortex, the blast wave becomes curved and keeps moving forward to interact with the normal shock as shown in the plots at t=1.7 msec. At t=1.9 msec, the flow pattern reveals that as a result of the interaction, the blast wave is broken into two parts while several new vortices are created. More complex flow patterns are shown at t=2.1 and 2.3 msec, describing further reflection and interaction of shock waves and vortices.

Despite the difference between 2-D and axisymmetric configurations, the computed flow fields agree extremely well with those shown in the shadowgraph pictures of Ref. 15 at early time steps of t=0.1996 and 0.4937 msec. An axisymmetric Euler solver based on the CE/SE method is being developed, which will be used to simulate the realistic experimental flow conditions.

3. Conclusions

The 1-D, quasi 1-D and 2-D Euler solvers have been validated using test problems. Numerical examples have been used to compare the CE/SE Euler solvers with established schemes such as the TVNI schemes designed by Harten, the upwind schemes used by Woodward and Colella, and others. It has been demonstrated that the present Euler solvers can generate highly accurate numerical solutions without requiring any special treatments for flow discontinuities, such as the inclusion of artificial viscosity, blending of low- and high-order-accurate fluxes, the use of nonlinear solution to Riemann's problem as suggested in Ref. 10, or the TVD property used in Ref. 15. Its inherent features of simplicity, generality and accuracy indicate that, with further improvements, the space-time conservation element and solution element method may be developed to become a versatile tool for solving general fluid dynamic problems.

Acknowledgment

This work was supported by NASA Lewis Research Center through Grant NAG3-1566.

References

[1]Chang, S.C., "The Method of Space-Time Conservation Element and Solution Element — A New Approach for Solving the Navier-Stokes and Euler Equations," *Journal of Computational Physics*, Vol. 191, 1995, pp. 295-324.

[2]Chang, S.C., Wang, X.Y., and Chow, C.Y., "New Developments in the Method of Space-Time Conservation Element and Solution Element — Applications to Two-Dimensional Time-Marching Problems," NASA TM-106758, December, 1994.

[3]Wang, X.Y., Chow, C.Y., and Chang, S.C., "High Resolution Euler Solvers Based on the Space-Time Conservation Element and Solution Element Method," to appear as a NASA TM.

[4]Wang, X.Y., Chow, C.Y., and Chang, S.C., "Application of the Space-Time Conservation Element and Solution Element Method to Shock-Tube Problem," NASA TM-106806, December, 1994.

[5]Harten, A., "High Resolution Schemes for Hyperbolic Conservation Laws," *Journal of Computational Physics*, Vol. 49, No. 3, 1983, pp. 357–393.

[6]Einfeldt, B., Munz, C.D., Roe, P.L., and Sjögreen, B., "On Godunov-Type Methods near Low Densities," *Journal of Computational Physics*, Vol. 92, No. 2, 1991, pp. 273–295.

[7]Xu, K., Martinelli, L., and Jameson, A., "Gas-Kinetic Finite Volume Method, Flux-Vector Splitting and Artificial Diffusion," *Journal of Computational Physics*, Vol. 120, No. 1, 1995, pp. 48–65.

[8]Shu, C.W., and Osher, S., "Efficient Implementation of Essentially Non-Oscillatory Shock-Capturing Schemes, II," *Journal of Computational Physics*, Vol. 83, No. 1, 1989, pp. 32–78.

[9]Huynh, H.T., "Accurate Upwind Schemes for the Euler Equations," AIAA-95-1737-CP, June, 1995.

[10]Woodward, P., and Colella, P., "The Numerical Simulation of Two-Dimensional Fluid Flow with

Strong Shock," *Journal of Computational Physics*, Vol. 54, No. 1, 1984, pp. 115–173.

[11]Liou, M.S., "Progress Towards an Improved CFD Method: AUSM$^+$," AIAA-95-1701-CP, June, 1995.

[12]Shubin, G.R., Stephens, A.B., and Glaz, H.M., "Steady Shock Tracking and Newton's Method Applied to One-Dimensional Duct Flow," *Journal of Computational Physics*, Vol. 39, No. 2, 1981, pp. 364–374.

[13]Giannakouros, J., and Karniadakis, G.E., "A Spectral Element–FCT Method for the Compressible Euler Equations," *Journal of Computational Physics*, Vol. 115, No. 1, 1994, pp. 65–85.

[14]Van Leer, B., "Towards the Ultimate Conservative Difference Scheme. V. A Second-Order Sequel to Godunov's Method," *Journal of Computational Physics*, Vol. 32, 1979, pp. 101–136.

[15]Wang, J.C.T., and Widhopf, G.F., "Numerical Simulation of Blast Flowfields Using a High Resolution TVD Finite Volume Scheme," AIAA Paper 87-1320, June, 1987.

Fig. 1 The CE/SE solution for Lax problem
(CFL=0.95, ΔX=0.1, a=4, t=100Δt)

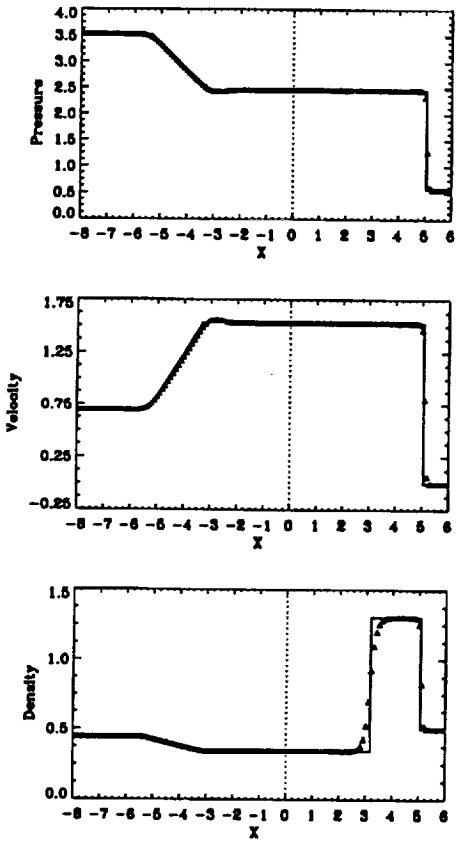

Fig. 2 The CE/SE solution for Sjogreen problem
(Δt=0.002, ΔX=0.01, a=1, t=50Δt)

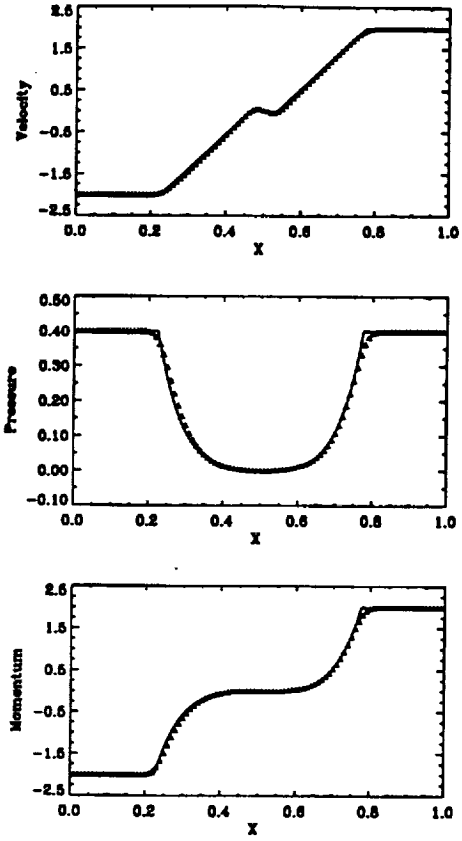

Fig. 3 The CE/SE solution for Shu–Osher problem
(Δt=0.0015, ΔX=0.0125, a=1, t=1.8)

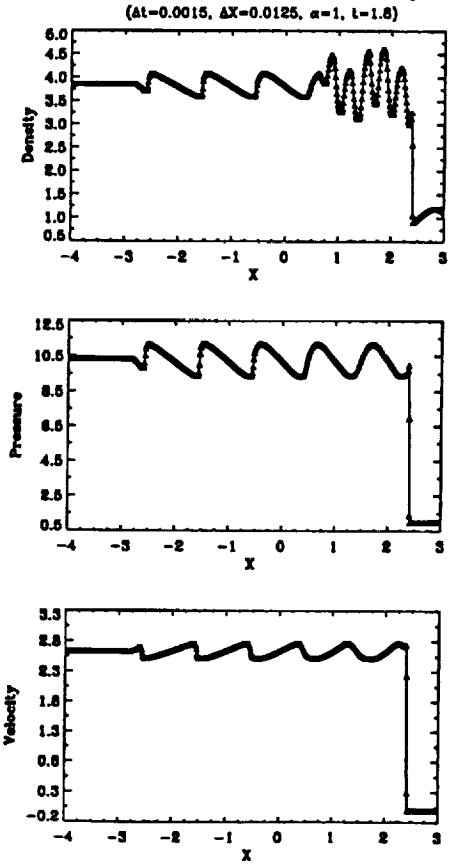

Fig. 4 The CE/SE solution for blast wave problem

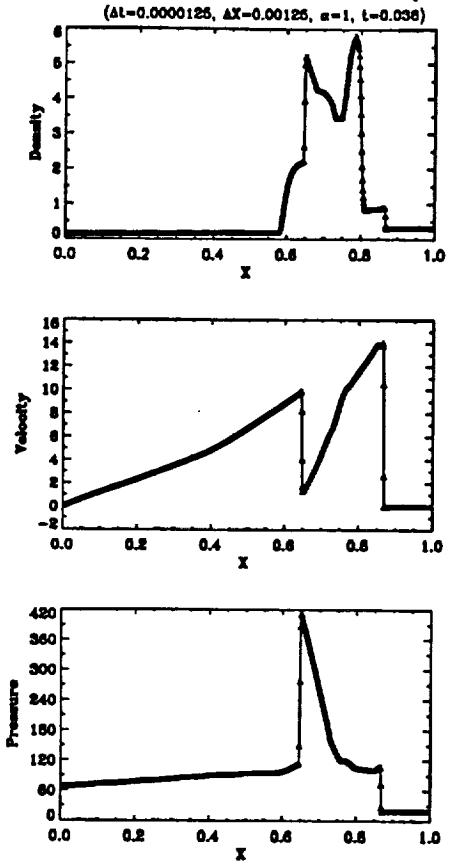

Fig. 5 The CE/SE steady-state solution of nozzle probelm

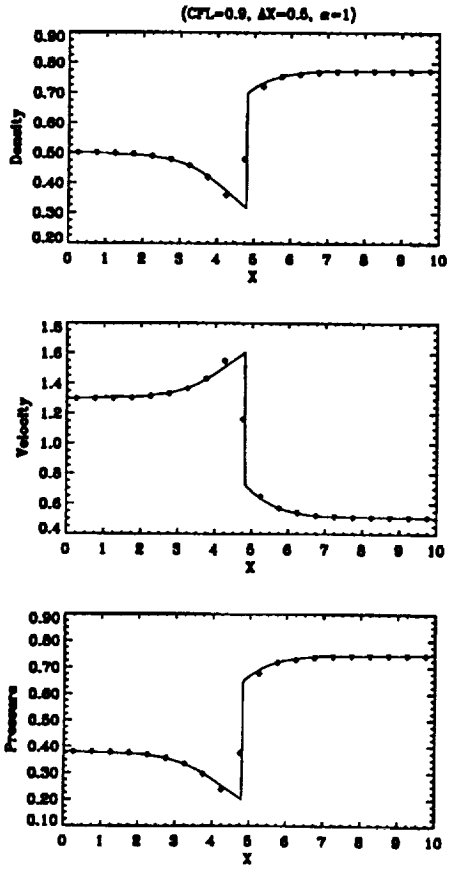

Fig. 6 The CE/SE steady-state solution of nozzle probelm

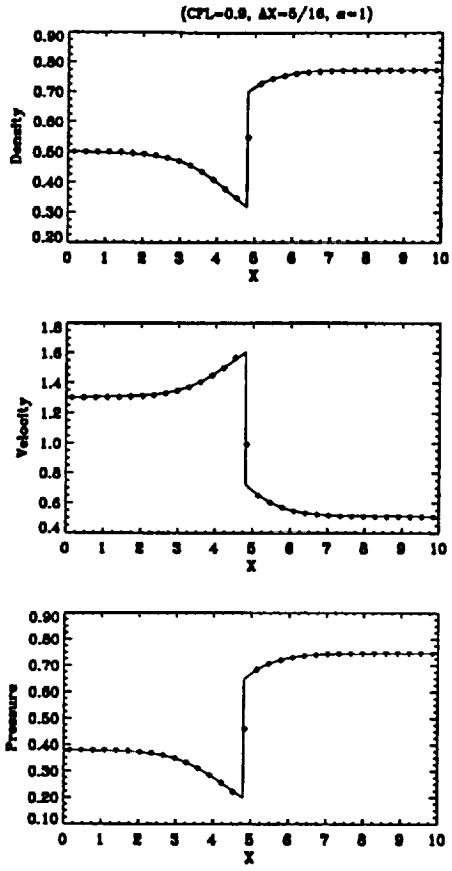

Fig. 7(a) Geometry of the duct with a step

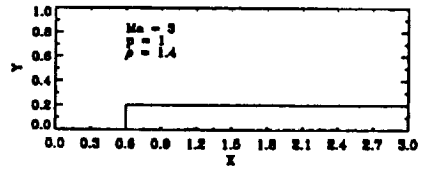

Fig. 7(b) Grid distribution in the duct

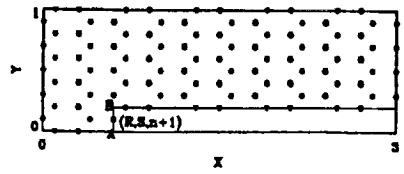

Fig. 8 Density contours for flow over a step at t=4

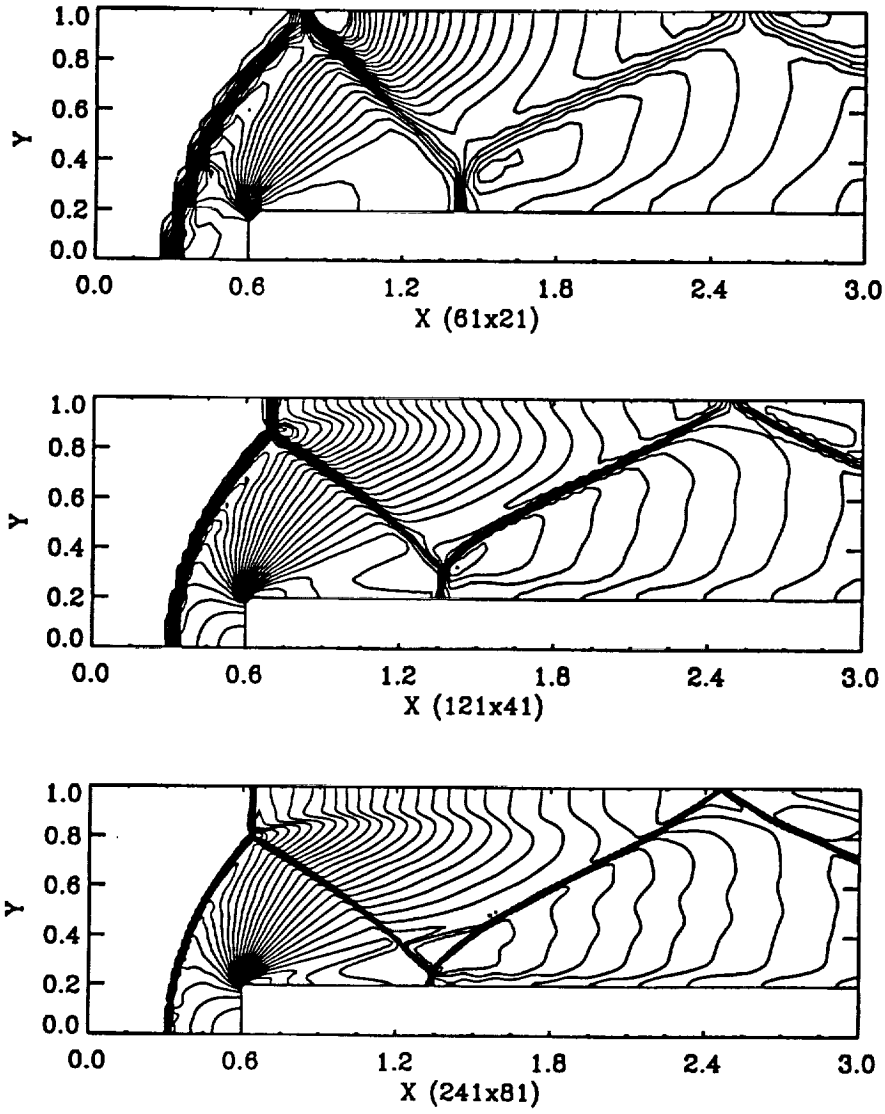

Fig. 9 Grid distribution in the blastfield

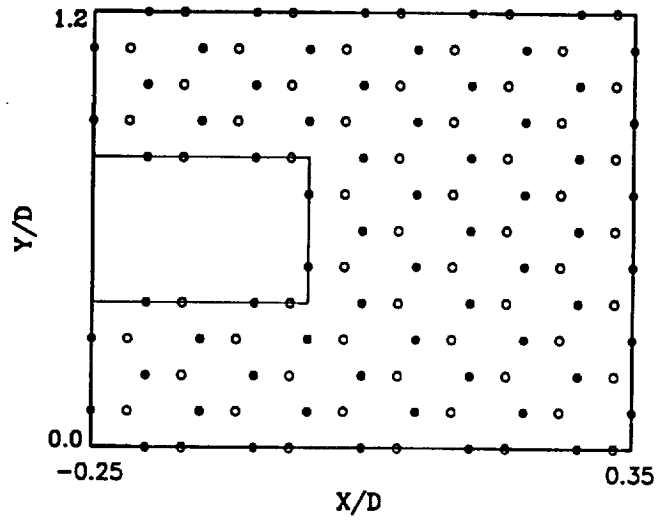

Fig. 10 Locus of vortex center

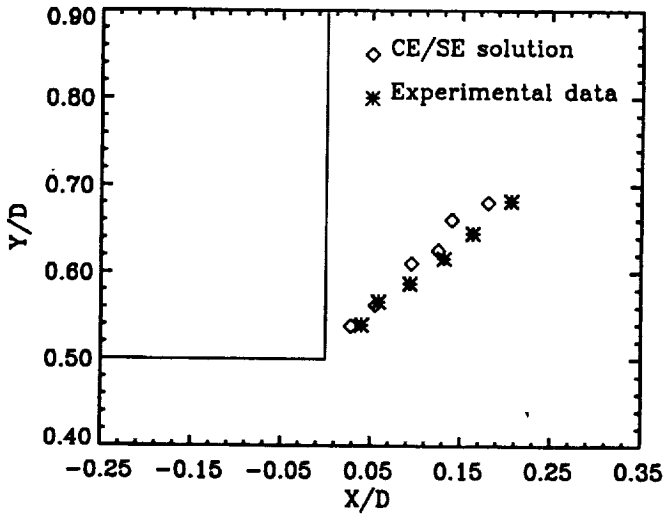

Fig. 11 Velocity vector plots at early times

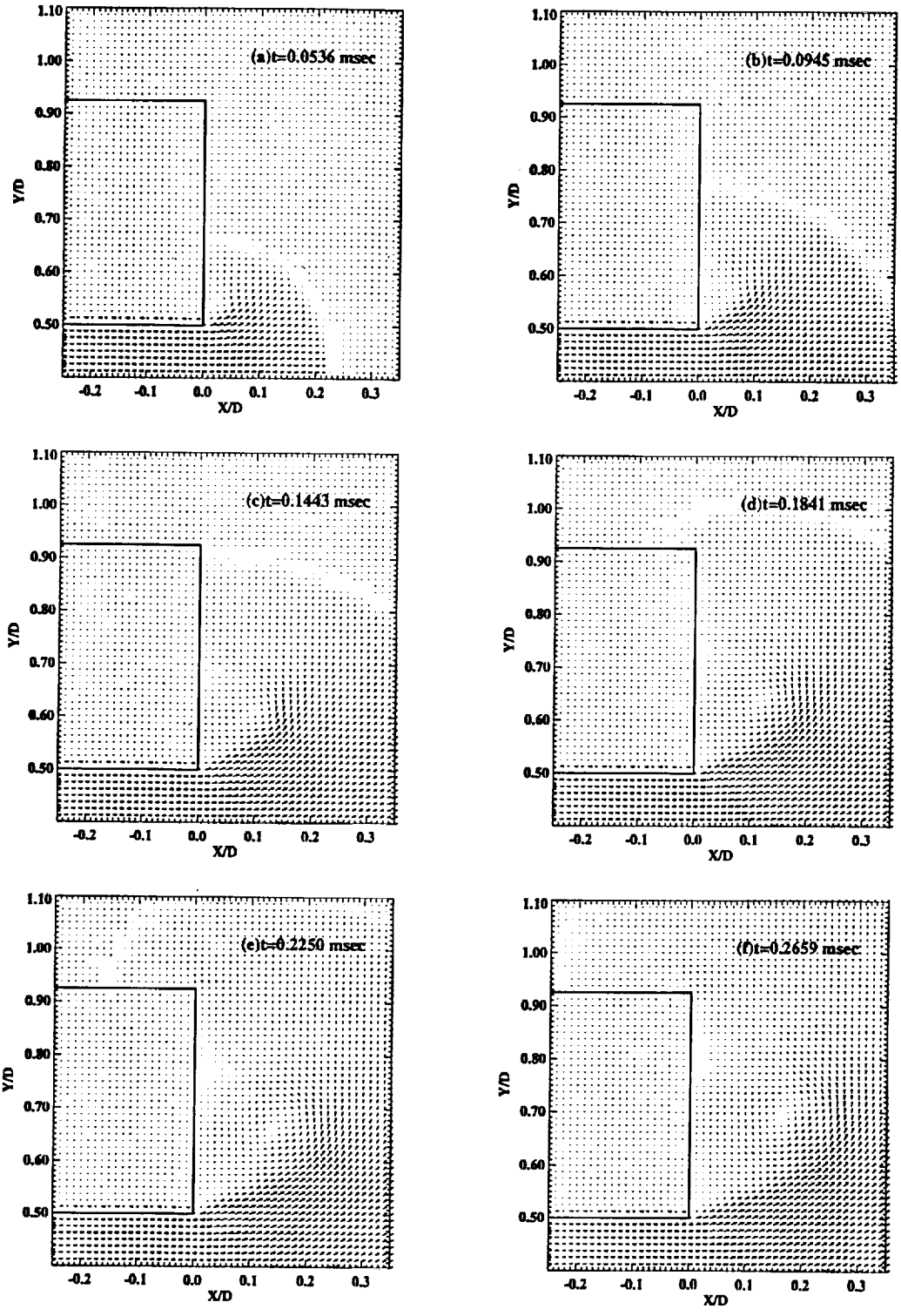

Fig. 12 Pressure contours at eight time levels

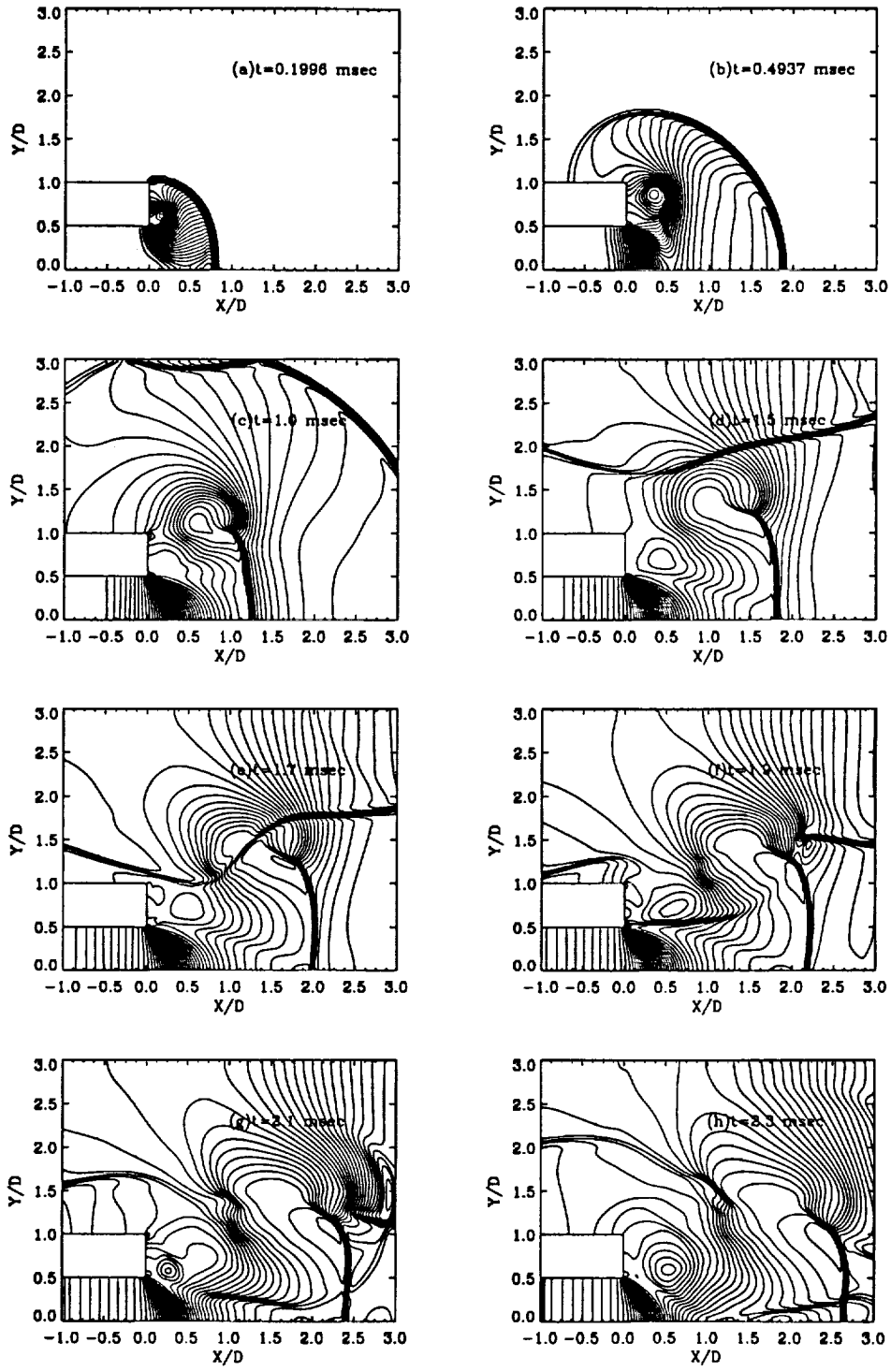

Fig. 13 Density contours at eight time levels